International Journal of Nanomedicine

Dovepress
open access to scientific and medical research

Open Access Full Text Article

ORIGINAL RESEARCH

Triple-functional albumin-based nanoparticles for combined chemotherapy and photodynamic therapy of pancreatic cancer with lymphatic metastases

This article was published in the following Dove Press journal:
International Journal of Nanomedicine
12 September 2017
Number of times this article has been viewed

Xinzhe Yu[1]
Wenwen Zhu[2]
Yang Di[1]
Jichun Gu[1]
Zhongyi Guo[1]
Hengchao Li[1]
Deliang Fu[1]
Chen Jin[1]

[1]Department of Pancreatic Surgery, Huashan Hospital, Fudan University, Shanghai, [2]Institute of Functional Nano & Soft Materials, Collaborative Innovation Center of Suzhou Nano Science and Technology, Soochow University, Suzhou, Jiangsu, China

Abstract: Lymphatic metastasis is the major metastatic pattern of pancreatic cancer and considered as an independent risk factor of survival. However, there is still no effective way for the diagnosis and treatment for lymphatic metastases of pancreatic cancer. In this study, using albumin as a carrier of gemcitabine (Gem), further modified by pyropheophorbide-a, we have designed and synthesized a nanoparticle (NP) compound named "pheophorbide-a (P@)-Gem-human serum albumin (HSA)-NPs". By utilization of its tracer ability of lymphatic metastases, which is triggered by near-infrared irradiation and its visible dying ability, the compound is used for drug delivery tracking, meanwhile as a treating drug, as well as the combined effect of photodynamic therapy and chemotherapy. By the nude mice model of lymphatic metastases of pancreatic cancer (BxPC-3-LN7), we aim to explore the feasibility, effectiveness, and biological safety of diagnosis and treatment for the lymphatic metastases of pancreatic cancer by P@-Gem-HSA-NP, thereby, providing new methods and strategies for the study of nanodrug carrier and research on lymphatic metastases of pancreatic cancer.

Keywords: theranostic nanoparticles, chemotherapy, photodynamic therapy, pancreatic cancer, lymphatic metastases, near infrared irradiation

Introduction

Pancreatic cancer is the fourth leading cause of cancer-related death in America, and its 5-year survival rate is <5%.[1,2] Although surgery is the only way to cure, only 20% of patients are eligible for this approach at the time of diagnosis.[3] Furthermore, a variety of these resectable patients will experience recurrence or metastases after radical surgery. Therefore, chemotherapy is the only option for these advanced pancreatic cancer patients.[4] Lymph node metastasis is the main metastatic pattern of pancreatic cancer, which directly leads to the cancer death.[5] Therefore, it is of vital importance to identify new strategy to locate the sentinel lymph node (SLN), which is the first target in early-stage cancer metastases, and then eradicate metastatic cancer cells in this SLN to prevent further cancer metastases.[6–8]

Theranostic nanomedicine, being capable of diagnosis, therapy, and monitoring drug delivery and distribution, has received growing interests recently.[9–12] Up to now, multifunctional nanoparticles (NPs) in the field of anticancer, such as the combination of diagnosis and therapy, have been intensively developed and achieved great significances.[13–16] Among abundant combination choices, "photodynamic therapy

Correspondence: Chen Jin
Department of Pancreatic Surgery, Huashan Hospital, Fudan University, Middle Urumqi Road 12#, Shanghai 200040, China
Tel +86 136 0198 1174
Email galleyking@hotmail.com

submit your manuscript | www.dovepress.com
Dovepress
http://dx.doi.org/10.2147/IJN.S131295

(PDT) plus chemotherapy" has been shown to be an effective modality to provide synergistic and complementary interactions between different treatments.[17] Zhang et al designed and prepared a self-monitored and self-delivered photosensitizer (PS)-doped fluorescence resonance energy transfer NP drug delivery system. By exploiting the emitters, the combinatorial drug can achieve chemotherapy, PDT, and real-time self-monitoring of the release and distribution of the nanomedicine. As expected, the as-prepared NPs showed high cancer therapeutic efficacy both in vitro and in vivo.[18]

Currently, gemcitabine (Gem) (2′,2′-difluoro-2′-deoxycytidine) is recommended as the first-line regimen for pancreatic cancer.[19,20] However, due to low molecular weight and high solubility in water, the clinical benefits of Gem are compromised by its short plasma half-life and relative low concentration around tumor sites.[20] In previous work,[21] we have reported using NP albumin-bound (Nab) technique to prepare Gem-loaded human serum albumin (HSA) NPs (Gem-HSA-NPs), which exhibited satisfied inhibition effect with moderate toxicity both in vitro and in vivo. However, this single therapeutic approach remains compromising for completely curing cancer.[22,23] In addition, lack of real-time monitoring of drug delivery may lead to overdose or under-dose.[24–26] Notably, developing a self-monitored drug delivery system may facilitate personalizing therapeutic modalities for treatment guidance as well as assessing the response to therapy.[27–29] PDT involves the administration of PS and is then irradiated under near infrared (NIR) to induce cell death. The overall reaction generates reactive oxygen species, such as singlet oxygen ($^1O_2$) and free radicals, which are toxic and would be able to kill cancer cells.[30] However, many applied PS molecules are hydrophobic and tend to aggregate easily in aqueous media, leading to a decrease in its quantum yield and problems for intravenous administration.[31,32] Pheophorbide-a (P@) is a second-generation PDT agent with a high singlet oxygen quantum yield and a high extinction coefficient in the NIR region.[33,34] However, its clinical applications of PDT are greatly inhibited due to the poor water solubility character. Albumin, a versatile protein carrier for the drug delivery, has been shown to be biocompatible, biodegradable, and nontoxic.[35,36] In addition, its unique structure makes it easy to conjugate with both hydrophobic and hydrophilic materials.[37] Therefore, we wonder if we could use albumin as drug carrier, on the other hand, by conjugating with P@ and generating NPs to increase water solubility as well as controlled release character, thus achieving imaging-guided combined PDT and chemotherapy effect.

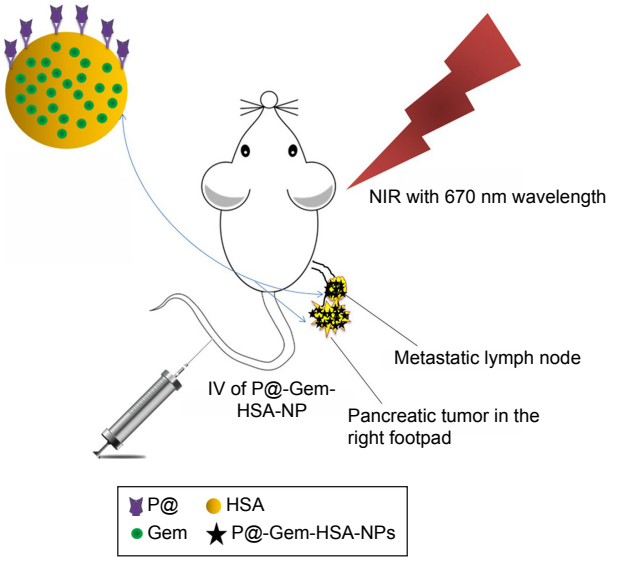

Figure 1 A schematic illustration showing the composition of this triple-functional NP.
Notes: Gem was binding with or encapsulated by HSA, and the outer layer of HSA was conjugated with P@. After IV of P@-Gem-HSA-NPs via the tail vein, the concept of theranostic through imaging-guided combined PDT and chemotherapy toward pancreatic cancer with lymphatic metastases is exhibited.
Abbreviations: Gem, gemcitabine; HSA, human serum albumin; IV, intravenous injection; NIR, near infrared; NPs, nanoparticles; P@, pheophorbide-a; PDT, photodynamic therapy.

In this work, we have successfully developed triple-functional albumin-based NPs by encapsulating Gem into P@-conjugated HSA, named P@-Gem-HSA-NPs. As shown in Figure 1, these well-designed NPs could efficiently accumulate into the tumor site and metastatic lymph nodes via the enhanced permeability and retention (EPR) effect.[38–40] Under NIR irritation, the PS P@ can produce optical fluorescence, which is used for the early diagnosis and tracking drug delivery. In addition, the released Gem as well as P@ will contribute a combined PDT and chemotherapy effect. Through strong evidences from in vitro and in vivo tests, we firmly believe that this imaging-guided theranostic NP offers great potential toward pancreatic cancer with lymphatic metastases, which will open exciting opportunities for biomedical applications.

Materials and methods

Materials

Gem was purchased from Eli Lilly and Company (Indianapolis, IN, USA). The Gem-C14 was prepared as before.[41] HSA (20%, 50 mL) was purchased from the Baxter International Inc. (Deerfield, IL, USA). P@ was obtained from the Shanghai Dibo Chemical Agent Co., Ltd. (Shanghai, China); (1-ethyl-3-(3-dimethylaminopropyl) carbodiimide hydrochloride) (EDC) and N-Hydroxysuccinimide (NHS) were obtained from Thermo Fisher Scientific (Waltham, MA, USA). Normal saline (NS) was purchased from Shanghai Baxter

Healthcare Co., Ltd. (Shanghai, China). Absolute ethanol and chloroform were purchased from Sinopharm Chemical Reagent Co., Ltd. (Shanghai, China). Deionized water was purchased from Fudan University (Shanghai, China). Roswell Park Memorial Institute (RPMI)-1640 culture medium and fetal bovine serum (FBS) were obtained from Thermo Fisher Scientific. Hoechst 33342 was purchased from Sigma-Aldrich Co. (St Louis, MO, USA). Cell Counting Kit-8 (CCK-8) was purchased from Dojindo (Kyushu, Japan). Terminal deoxynucleotidyl transferase dUTP nick end labeling (TUNEL) kit was purchased from Hoffmann-La Roche Ltd. (Basel, Switzerland). Phosphate buffered solution (PBS) and other reagents were prepared in our laboratory. All the solvents and chemicals were of analytical grade. The PDT treatment both in vivo and in vitro was conducted by a 670 nm laser (Hi-Tech Optoelectronics Co., Ltd., Beijing, China).

Preparation of P@-HSA

Activation of P@ for reaction with HSA

P@, EDC, and NHS were dissolved in 30 mL anhydrous dimethylformamide (DMF) and then added to 300 mL of PBS buffer (0.1 M KH_2PO_4, 0.1 M Na_2HPO_4, 0.9 M NaCl, pH 7.8), and the mixture was stirred for 30 min at room temperature. After the reaction, a defined amount of 2-mercaptoethanol was added to quench the excessive EDC.

Added activated P@ to HSA

Molar ratios of HSA to P@ in the final conjugation reaction were 1:34. Briefly, the HSA was dissolved with 250 mL of PBS buffer (pH 7.8), and then the mixture was added slowly to the HSA PBS buffer. The reaction could proceed under constant agitation for 5 h under a nitrogen atmosphere, and the mixture was on dialysis in PBS buffer at 4°C and then freeze-dried with the lyophilizer.

Synthesis of P@-Gem-HSA-NPs

The P@-Gem-HSA-NPs were prepared by the Nab technology as previously reported.[21] Briefly, P@-HSA was mixed with pure water. Separately, Gem-C14 was dissolved in chloroform saturated with pure water. These two solutions were then fully mixed and homogenized (Nano DeBEE manufactured by BEE International, South Easton, MA, USA) at 20,000 psi for nine cycles. The generated colloid was rotary evaporated to remove chloroform at 25°C for 15 min under vacuum. The obtained NPs were then filtered through a 0.25 μm membrane syringe filter, and the solvent was removed by lyophilization for 48 h after being frozen at −80°C. The obtained P@-Gem-HSA-NPs' powder was vacuum dried for 48 h and stored at room temperature.

Characterization

The particle size and zeta potential were determined using Zetasizer (Malvern Instruments, Malvern, UK) at a scattering angle of 120°. The NP suspension was added drop wise onto the copper grids, which was then dried at room temperature. Transmission electron microscopy (TEM) images of the NPs were acquired under 20,000× and 50,000× magnification (H-600; Hitachi Ltd., Tokyo, Japan).

To determine the drug-loading efficiency and encapsulation efficiency, a preweighed aliquot of P@-Gem-HSA-NPs/Gem-HSA-NPs was placed in DMF solution and sonicated to extract the Gem-C14. The extracted Gem-C14 was analyzed by ultraviolet–visible spectroscopy (UV–vis) spectrophotometer. Data were collected, and the efficiencies were calculated using the following formulas:

$$\text{Encapsulation efficiency (\%)} = \frac{\text{Weight of Gem} - \text{C14 encapsulated}}{\text{Weight of Gem} - \text{C14 fed initially}} \times 100$$

$$\text{Drug loading efficiency (\%)} = \frac{\text{Weight of Gem} - \text{C14 loaded}}{\text{Weight of P@} - \text{Gem-HSA-NPs}} \times 100$$

UV–vis–NIR spectra were acquired using a Lambda 750 UV–vis spectrophotometer (PerkinElmer Inc., Waltham, MA, USA). The generation of singlet oxygen was determined by the singlet oxygen sensor green (SOSG) dye following the standard procedure. The amount of entrapped Gem-C14 was determined by UV–vis spectrophotometer. The Gem-C14 release test was performed in 180 mL of PBS at pH 7.4. P@-Gem-HSA-NPs and Gem-HSA-NPs (10 mg) were resuspended in 10 mL PBS and loaded in a dialysis bag. The release system was swayed in a bath reciprocal shaker at 100 rpm and at a constant temperature of ≥37°C for 120 h. Aliquots (2 mL) were extracted at desired time intervals, and another 2 mL fresh PBS was added to the system. The accumulated amount of Gem-C14 released was determined by UV–vis spectrophotometer.

Cellular experiments

Cell culture

The BxPC-3 cell line (human pancreatic cancer, originally from American Type Culture Collection) was purchased from the Shanghai Branch of the Chinese Academy of Sciences (Shanghai, China).

Cells were cultured at 37°C in the presence of 5% CO_2 and 95% air with >95% humidity. Cells were grown in RPMI-1640 containing 10% FBS, 100 U/mL penicillin, and 100 mg/mL streptomycin.

Cellular uptake experiments

The BxPC-3 cells were seeded in six-well plates at a density of 1×10^4 cells/well. After incubation with NS, P@, and P@-Gem-HSA-NPs for 4 h, cells were washed with PBS and fixed in paraformaldehyde for 10 min, followed by cell nuclei staining with 4′,6-diamidino-2-phenylindole (DAPI) for 10 min. Cover slips were mounted on slides after three washes with PBS, and the slides were analyzed by confocal microscopy (DMI 4000B; Leica Microsystems, Wetzlar, Germany).

Cell viability

The in vitro cytotoxic effects of Gem, Gem-HSA-NP, P@ without 670 nm light exposure (L–), P@ under 670 nm light exposure (L+, optical dose =3.6 J/cm^2, 5 min), P@-Gem-HSA-NPs without light exposure (L–), and P@-Gem-HSA-NPs under 670 nm light exposure (L+, optical dose =3.6 J/cm^2, 5 min) in the BxPC-3 cells were determined using the CCK-8 assay. Briefly, cells were seeded into 96-well culture plates (10,000 cells/well) and incubated overnight at 37°C, 5% CO_2. Then, the cells were incubated with various concentrations of Gem, Gem-HSA-NP, P@ (L–), P@ (L+), P@-Gem-HSA-NPs (L–), and P@-Gem-HSA-NPs (L+) for 48 h. Cell viability was quantitated based on the dye absorption at 450 nm, which was determined using an automatic multiwell spectrophotometer. The cell inhibition rate (%) was calculated as follows: [1 − (absorbance of the study group/absorbance of the control group)] × 100.

In vivo safety assessment

A total of 15 healthy C57BL/6 mice were allocated to three groups (n=5) and received intravenous injection (IV) of NS (control group), Gem, and P@-Gem-HSA-NPs (Gem equivalent: 100 mg/kg, twice as the dose of therapeutic level). For in vivo safety assessment, major organs, including the heart, liver, spleen, lung, and kidney, were harvested 10 days postinjection. Then, all tissues were fixed in 4% formalin, processed routinely into paraffin, sectioned into thin slices, and stained with hematoxylin and eosin (H&E) stain for histological analysis. Before sacrificing, bloods were collected for biochemistry assay and complete blood panel test at 10 days postinjection. The serum biochemistry data and complete blood panel were measured in Shanghai Biochemistry Institute.

Animal model

The C57BL/6 mice and BALB/c-nu/nu female mice (weighing 20±2 g) were purchased from the Charles River Laboratories (Wilmington, MA, USA) and housed in a pathogen-free animal facility. The temperature was maintained at 24°C with a humidity of 50%–60%, and the mice were subjected to a 10/14 h light/dark cycle. All animal studies were approved by the Institutional Animal Care and Use Committee of Fudan University, whose guidelines were in compliance with the approved animal care protocols.

A highly lymphatic metastatic pancreatic cancer cell line BxPC-3-LN7 was generated from BxPC-3 cells through a continuous in vivo screening and seeding method. The model for metastatic lymph nodes was established as previously reported by our group.[8] Studies were performed on these mice ~6 weeks after inoculation when the popliteal lymph nodes could be touched by hand.

In vivo and ex vivo imaging

In vivo real-time fluorescence mapping analysis was used to evaluate the effects of P@-Gem-HSA-NP accumulation in various tissues of tumor-bearing mice. Nine mice were randomized into three groups (n=3), in which the mice were injected with NS (100 μL), P@ (100 μL, 2 mg/mL), or P@-Gem-HSA-NPs (100 μL, equivalent P@ dosage). After 1, 2, 3, 4, 6, and 24 h, the mice were anesthetized and visualized using a Cambridge Research & Instrumentation in vivo imaging system (Hopkinton, MA, USA). To compare the ex vivo biodistribution of free P@ and P@-Gem-HSA-NPs in normal tissues, the mice were sacrificed after 24 h postinjection and each tissue was excised. The residual fluorescence intensity of P@ in each tissue was visualized with the same imaging system.

In vivo combined therapy

The animal model was obtained by subcutaneous injection of 1×10^7 BxPC-3-LN7 cells suspended in 100 μL RPMI-1640 medium via right-hind footpad of the nude mice. Studies were done about 2 weeks after implantation when the tumor diameter reached 5.0 mm. The PDT treatment was conducted by a 670-nm laser. Then, 30 mice were randomized into six groups (n=5), and each group was treated with 100 μL of NS, Gem, P@ (L+, irradiated by 670 nm light, 10 mW/cm^2, treating for 1 h, 12 h postinjection), Gem-HSA-NP, P@-Gem-HSA-NPs (L–, without light irradiation), and P@-Gem-HSA-NPs (L+, irradiated by 670 nm light, 10 mW/cm^2, treating for 1 h, 12 h postinjection) through tail vein injection on day 0 (Gem or equivalent dosage: 50 mg/kg body weight). Body weights and tumor sizes of mice were monitored for every 2 days. Tumor volume was estimated by using the formula: volume (mm^3) = (length in millimeter) × (width in millimeter)^2/2.

Tissue assays

On day 1 post-IV administration, the mice were anesthetized followed by heart perfusion with PBS (pH =7.4). After

scarified, the tumor mass was harvested, photographed, and then fixed with paraformaldehyde for 48 h and embedded in paraffin. Each section was cut into 5 μm and used for TUNEL staining according to the manufacturer's instructions. Nuclei staining was performed with DAPI (blue) to locate the nucleus, which upon the percentage of apoptotic-positive (red stained) cells was visualized under confocal microscope (DMI 4000B). For H&E staining, the slices were dehydrated with 15% sucrose until subsidence and dehydrated further with 30% sucrose until subsidence. The slices were counterstained with 1 μL/mg Hoechst 33342 for 10 min at room temperature, and the distribution of fluorescence signals was analyzed with a confocal microscope (710; Carl Zeiss Meditec AG, Jena, Germany).

Statistical analysis

All the data were presented as the mean ± standard deviation (SD). Significant differences between two groups were determined using Student's *t*-test, while multiple groups were analyzed by one-way analysis of variance with Fisher's least significant difference. All the statistical analyses were performed using the SPSS software (version 22.0; IBM Inc., New York, NY, USA). A value of $p<0.05$ was considered significant.

Results and discussion

In order to obtain a Gem prodrug with satisfactory lipophilicity for albumin encapsulation, we designed and synthesized 4-*N*-myristoyl-(C14) Gem derivatives named Gem-C14 as before.[41] After analyzed by ^{1}H NMR, Gem-C14 had a purity of >99.9%. ^{1}H NMR (DMSO-d_6, 400 MHz) δ: 11.0 (1H, s), 8.25 (1H, d, *J*=7.5 Hz), 7.29 (1H, d, *J*=7.5 Hz), 6.34 (1H, d, *J*=6.6 Hz), 6.17 (1H, t, *J*=7.5 Hz), 5.32 (1H, brs), 4.20 (1H, m), 3.88 (1H, m), 3.83 (1H, m), 3.65 (1H, m), 2.39 (2H, t, *J*=7.2 Hz), 1.54 (2H, m), 1.24 (20H, brs), and 0.85 (3H, t, *J*=7.2 Hz).

The P@-Gem-HSA-NPs were formulated based on the Nab technology, in which Gem-C14 was mixed with P@-HSA in an aqueous solvent and passed under high pressure through a jet to form drug albumin NPs. We then characterized the obtained P@-Gem-HSA-NPs using Zetasizer and measured the size and surface charge of the complex at various weight ratios. Overall, the NPs showed a narrow size distribution and good water solubility. As shown in Figure 2A, the average size of the NPs was 165±15 nm and the PDI was 0.21±0.02. The NPs showed a negative surface potential of –35.8±25.5 mV (Figure 2B), indicating a good dispersity and stability in human

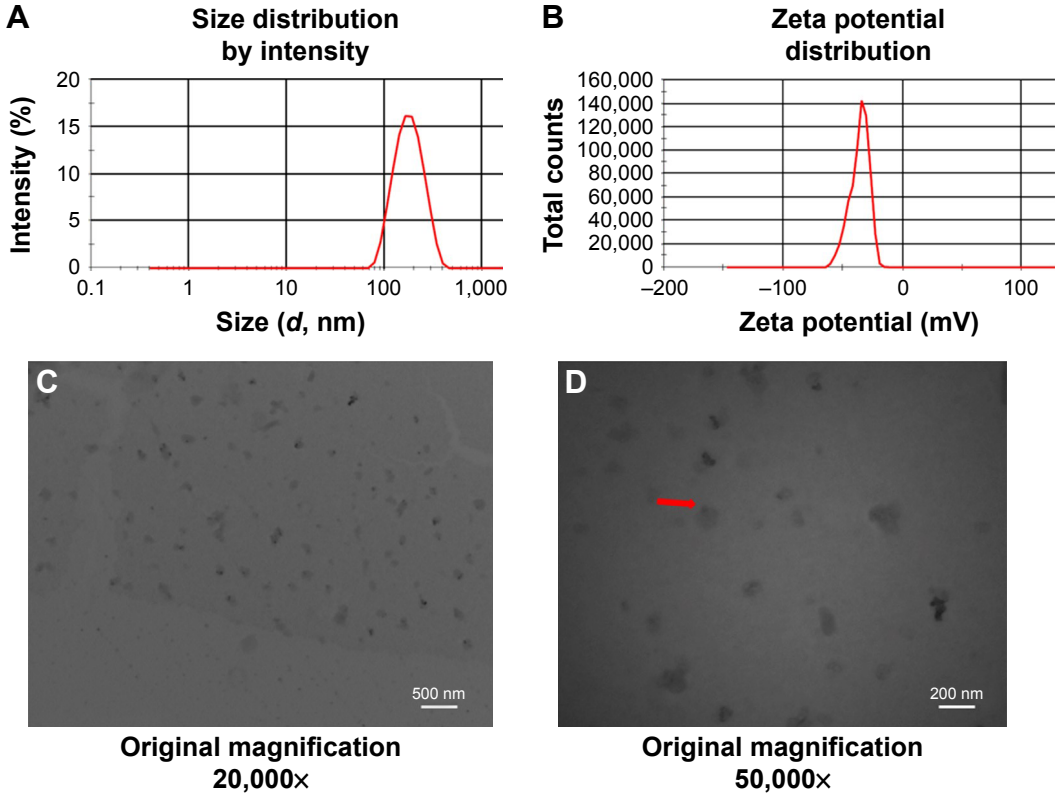

Figure 2 Characterization of P@-Gem-HSA-NPs.

Notes: (**A**) Average particle size and size distribution of P@-Gem-HSA-NPs. (**B**) Zeta potential spectrum of P@-Gem-HSA-NPs in PBS solution. (**C**) A TEM image of P@-Gem-HSA-NPs under 20,000× magnification. (**D**) A TEM image of P@-Gem-HSA-NPs under 50,000× magnification. The red arrow indicates the morphology of P@-Gem-HSA-NPs.

Abbreviations: Gem, gemcitabine; HSA, human serum albumin; NPs, nanoparticles; P@, pheophorbide-a; TEM, transmission electron microscopy.

blood, which may be conductive to a prolonged blood circulation. The encapsulation efficiency of P@-Gem-HSA-NPs was 93.61%±4.9%, while the drug-loading efficiency was 13.34%±2.2%. The morphology of the P@-Gem-HSA-NPs was observed by TEM. Under 20,000× magnification, the P@-Gem-HSA-NPs exhibited a nearly spherical shape with a moderately uniform particle size and an even distribution (Figure 2C). Under 50,000× magnification, the TEM image was likely to reveal the layer of NP surface, which was conjugated with P@ (the darker part). The particle size of P@-Gem-HSA-NPs estimated from TEM image was ~150 nm, which was similar to the result measured by Zetasizer (Figure 2D).

Next, we studied the optical properties of the P@-Gem-HSA-NPs. Under room temperature, the NPs showed a black powder status and good water solubility in PBS (Figure 3A). Then, the UV–vis–NIR absorption and fluorescence spectra of P@, P@-HSA, and P@-Gem-HSA-NPs were recorded. As indicated in Figure 3B, both P@-HSA and P@-Gem-HSA-NPs retained the characteristic absorption peak of P@ (670 nm). As expected, P@-Gem-HSA-NPs were found to be an effective PDT agent under 670 nm NIR laser irradiation. In contrast, to further verify the use of P@-Gem-HSA-NPs for PDT, we measured the $^1O_2$ production under excitation of the 670 nm light by a singlet oxygen sensor green based on its fluorescence recovery in the presence of $^1O_2$ (Figure 3C). It was found that PBS did not generate $^1O_2$ at all, while P@-Gem-HSA-NPs could effectively produce $^1O_2$ under light exposure, although its efficiency showed a slight decrease compared to the free P@. Therefore, the P@-Gem-HSA-NPs developed here could be utilized as potential agents for PDT. The in vitro release profiles of Gem-HSA-NPs and P@-Gem-HSA-NPs were recorded in a cumulative release curve for over 5 days. As shown in Figure 3D: initially both NPs exhibited an impulsive, fast-release profile, followed by a slow sustained release character. Overall, the P@-Gem-HSA-NPs showed good capping efficiency, controlled release character, and even higher release rate than the Gem-HSA-NPs, which may due to the interaction between P@ and the surface of NPs.

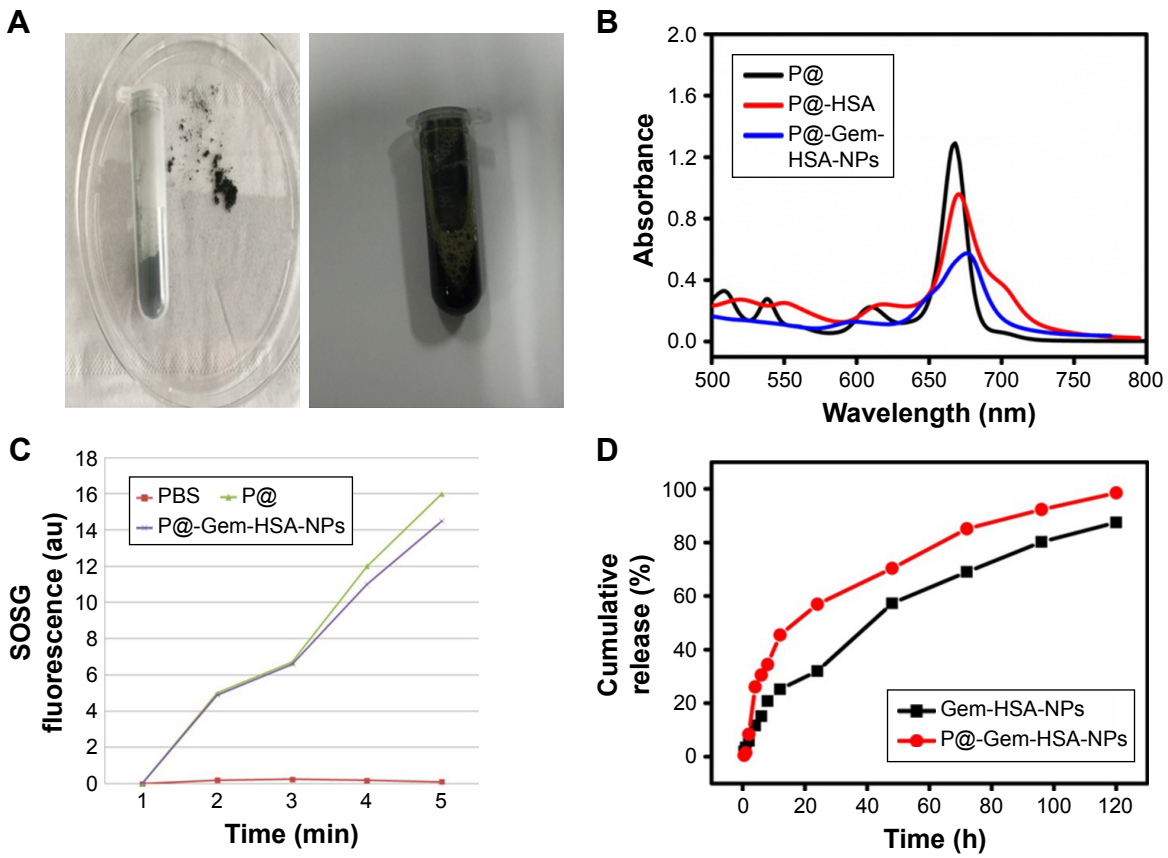

Figure 3 Characterization of P@-Gem-HSA-NPs.

Notes: (**A**) Optical properties of P@-Gem-HSA-NPs in powder and solution status. (**B**) UV–vis–NIR absorbance spectra of P@, P@-HSA, and P@-Gem-HSA-NPs in solution at the same concentration of P@. (**C**) Detection of singlet oxygen by the SOSG test of PBS, P@, and P@-Gem-HSA-NPs under NIR exposure with 670 nm wavelength for different periods of time. P@-Gem-HSA-NPs showed largely retained light-triggered SO generation ability compared to free P@ at the same P@ concentration. (**D**) The cumulative release profiles of Gem-HSA-NPs and P@-Gem-HSA-NPs.

Abbreviations: Gem, gemcitabine; HSA, human serum albumin; NIR, near infrared; NPs, nanoparticles; P@, pheophorbide-a; SO, singlet oxygen; SOSG, singlet oxygen sensor green; UV-vis, ultraviolet–visible spectroscopy.

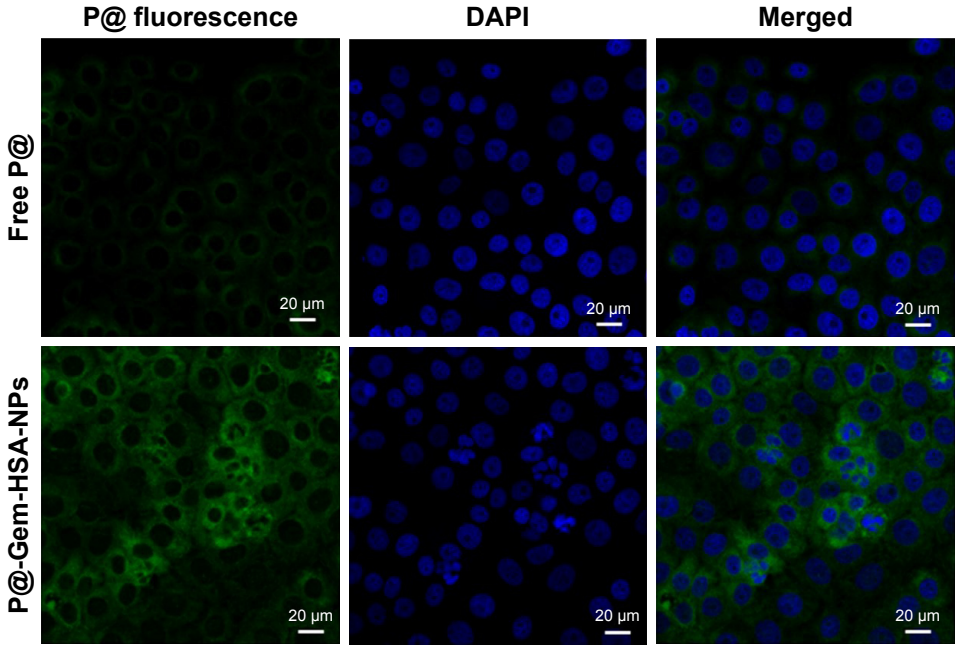

Figure 4 Confocal images of the BxPC-3 cells incubated with free P@ and P@-Gem-HSA-NPs.
Notes: Green: fluorescence of free P@ and P@-Gem-HSA-NPs. Blue: DAPI for BxPC-3 cell nucleus. Merged: fluorescence (green) and DAPI (blue). Bar: 20 μm; magnification ×500.
Abbreviations: DAPI, 4′,6-diamidino-2-phenylindole; Gem, gemcitabine; HSA, human serum albumin; NPs, nanoparticles; P@, pheophorbide-a.

Next, we would like to demonstrate the use of P@-Gem-HSA-NPs as theranostic agents for combined PDT and chemotherapy in vitro. We first studied the cellular uptake ability of P@-Gem-HSA-NPs by the confocal fluorescence microscopy. As shown in Figures 4 and S1, the BxPC-3 cells treated with P@-Gem-HSA-NPs exhibited significantly higher green fluorescence intensity than those treated with free P@. The combined effect of PDT and chemotherapy was then studied in vitro. In Figure 5, experimental points 0–5 corresponded to doses of 0, 0.08, 0.40, 2.00, 10.00, and 50.00 μg/mL, respectively. All testing groups inhibited cell growth in a dose-dependent manner. At various concentrations, P@-Gem-HSA-NPs (L+) exhibited the strongest cytotoxicity, whereas Gem group, P@ (L+) group, Gem-HSA-NPs group, and P@-Gem-HSA-NPs (L–) group showed similar inhibition manner, and P@ (L–) group indicated almost no cell killing ability. Compared to other singular treatment groups, P@-Gem-HSA-NPs (L+) showed a highly synergistic effect in destructing cancer cells by in vitro of combined PDT and chemotherapy ($P<0.05$).

One of the key concerns is the toxicity of NPs when applied in vivo.[42] Therefore, before in vivo combined therapy on mice model, we conducted in vivo safety assessment in healthy C57BL/6 mice. Notably, during the treatment process, all mice behaved normally after receiving various treatments. In the meanwhile, no noticeable sign of toxic side effect with P@-Gem-HSA-NPs was observed in our experiments, as revealed by histological examination of H&E-stained organ slices from P@-Gem-HSA-NP-injected mice collected 10 days postinjection (Figure 6). To further study the long-term toxicology of P@-Gem-HSA-NPs, serum

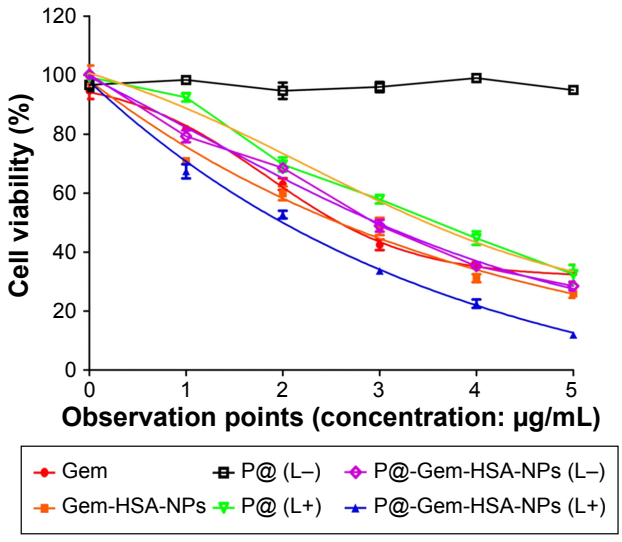

Figure 5 Cell viability of BxPC-3 cells after incubation with various treatments including Gem, Gem-HSA-NPs, P@ without 670 nm light exposure (L–), P@ under 670 nm light exposure (L+, optical dose =3.6 J/cm^2, 5 min), P@-Gem-HSA-NPs without light exposure (L–), and P@-Gem-HSA-NPs under 670 nm light exposure (L+, optical dose =3.6 J/cm^2, 5 min).
Note: The 0–5 surveying points indicated 0, 0.08, 0.40, 2.00, 10.00, and 50.00 μg/mL, respectively.
Abbreviations: Gem, gemcitabine; HSA, human serum albumin; NPs, nanoparticles; P@, pheophorbide-a.

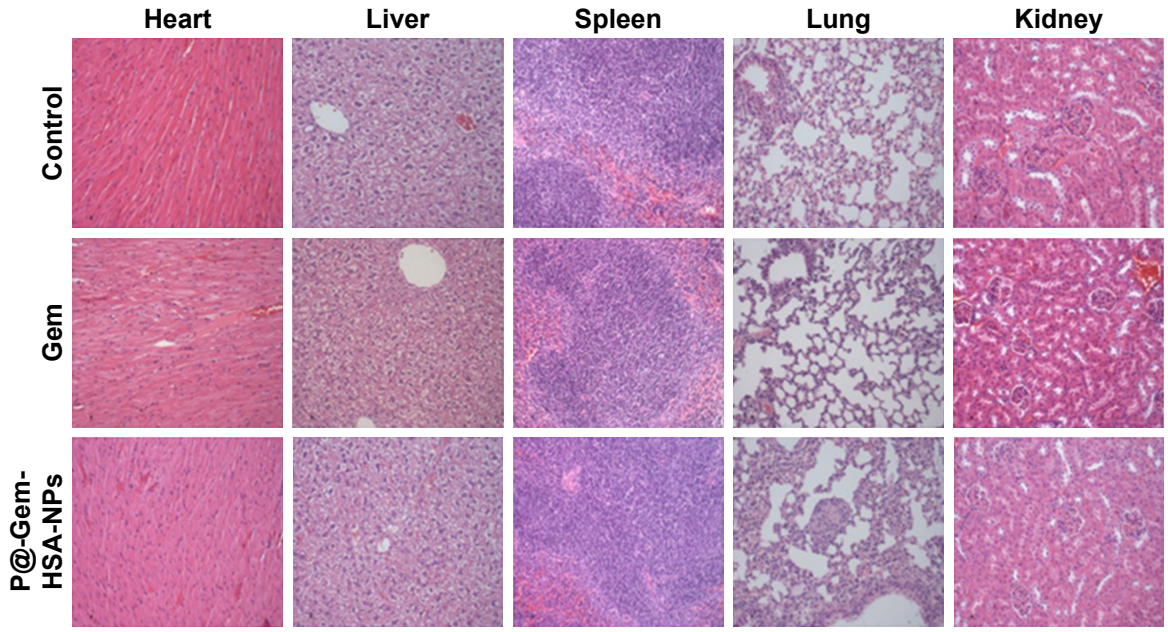

Figure 6 In vivo long-term toxicity of Gem and P@-Gem-HSA-NPs after intravenous injection (Gem equivalent: 100 mg/kg).
Notes: H&E-stained images of major organs (heart, liver, spleen, lung, and kidney) collected from healthy C57BL/6 mice treated by NS (control group), Gem, and P@-Gem-HSA-NPs under NIR irritation. All healthy C57BL/6 mice were injected with various treatments and sacrificed at 10 days post-IV for tissue assays Bar: 100 μm; magnification ×200.
Abbreviations: Gem, gemcitabine; H&E, hematoxylin and eosin; HSA, human serum albumin; IV, intravenous injection; NIR, near infrared; NPs, nanoparticles; NS, normal saline; P@, pheophorbide-a.

biochemistry assay and complete blood panel test were also carried out for P@-Gem-HSA-NP-injected healthy C57BL/6 mice at 10 days postinjection. As expected, all measured parameters fell within normal ranges (Table S1). It may be reasonable to predict that P@-Gem-HSA-NPs would not cause significant in vivo long-term toxicity.

Next, to demonstrate the potential for P@-Gem-HSA-NPs to visualize tumor tissues by NIR imaging, tumor-bearing mice were IV of P@-Gem-HSA-NPs through the tail vein. At the meantime, we also used P@ and NS as the positive and negative control groups, respectively. As shown in Figure 7, with widely distributed P@-Gem-HSA-NPs fluorescence

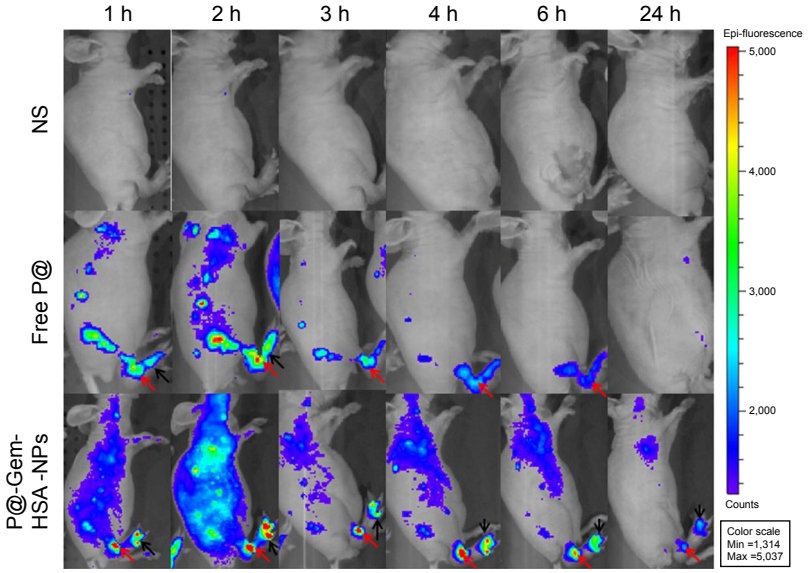

Figure 7 In vivo fluorescence images of pancreatic tumor-bearing mice taken at different time points post-IV of NS (control), free P@, and P@-Gem-HSA-NPs.
Note: Black arrows indicate pancreatic tumor in the right footpad, and the red arrows indicate metastatic popliteal lymph nodes.
Abbreviations: Gem, gemcitabine; HSA, human serum albumin; IV, intravenous injection; NPs, nanoparticles; NS, normal saline; P@, pheophorbide-a.

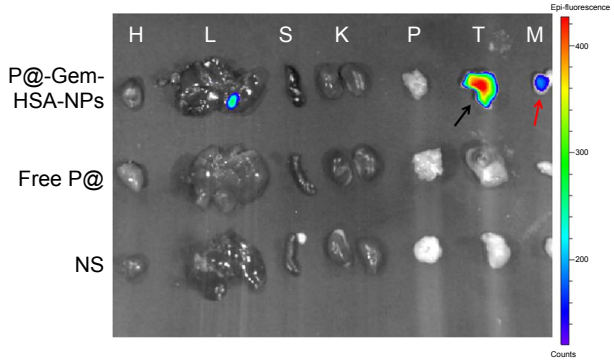

Figure 8 Ex vivo fluorescence images of major organs, tumors, and metastatic lymph nodes harvested from mice at 24 h postinjection.
Notes: H, L, S, K, P, T, and M indicated heart, liver, spleen, kidney, pancreas, tumor, and metastatic lymph nodes, respectively. The black arrow indicates pancreatic tumor in the right footpad, and the red arrow indicates metastatic popliteal lymph nodes.
Abbreviations: Gem, gemcitabine; HSA, human serum albumin; NP, nanoparticle; NS, normal saline; P@, pheophorbide-a.

at early time points, it was found that P@-Gem-HSA-NPs tended to be enriched in tumor tissues (pancreatic tumor in the right footpad and metastatic popliteal lymph nodes), with a peak uptake of NPs observed in the tumor at 4 h postinjection. Notably, at all observation points, the signal intensity of tumor tissues in P@-Gem-HSA-NPs group was significantly higher than that of free P@ group. Especially at 24 h postinjection, there was still strong signal in tumor and metastatic lymph nodes in the P@-Gem-HSA-NPs group, whereas in the P@ group, there was no signal left. The ex vivo fluorescence images also confirmed higher intensity at 24 h postinjection in the tumor tissues of the P@-Gem-HSA-NP-treated mice compared to that of the free P@-treated mice (Figure 8). These results clearly showed that P@-Gem-HSA-NPs effectively delivered P@ molecules into the tumor sites through the EPR effect.

Motivated by the high tumor and metastatic lymph node accumulation of P@-Gem-HSA-NPs, we then would like to use P@-Gem-HSA-NPs for in vivo combined PDT and chemotherapy. In our experiment, BxPC-3-LN7-bearing mice were randomly divided into six groups (n=5). The mice in each group were injected with NS, Gem, P@ (L+), Gem-HSA-NPs, P@-Gem-HSA-NPs (L–), and P@-Gem-HSA-NPs (L+), respectively. After 12 h postinjection, the mice in the (L+) group were irradiated with 670 nm light at a power density of 10 mW/cm^2 for 1 h (Figure S2), while the mice in the (L–) group were kept in dark environment. After various treatments, tumor volumes and body weights of mice in each group were monitored every other day. On day 14 posttreatments, all the mice in each group were sacrificed (Figure S3), and tumors as well as metastatic popliteal lymph nodes were harvested from each mouse (Figures 9A and B and 10A). During the entire study period, no mice died from any treatment-related cause. As shown in Figure 9C, although the weight profiles showed a sudden loss of 10%–20% until day 4 in the therapeutic group, they regained back to normal weight in the following days. As shown in Figure 9D, the tumor growth on mice in the NS group exhibited an uncontrollable manner, whereas in all treatment groups, tumors were inhibited to some extent. Remarkably, the tumor growth on mice treated with P@-Gem-HSA-NPs (L+) was almost completely inhibited. Furthermore, the metastatic lymph nodes in the P@-Gem-HSA-NPs (L+) group were also greatly inhibited (Figure 10B and C). To further understand the therapeutic efficacy after various treatments, H&E staining assays were introduced to study the morphology of tumor cells. The tumor slices of each group 1 day after treatments were

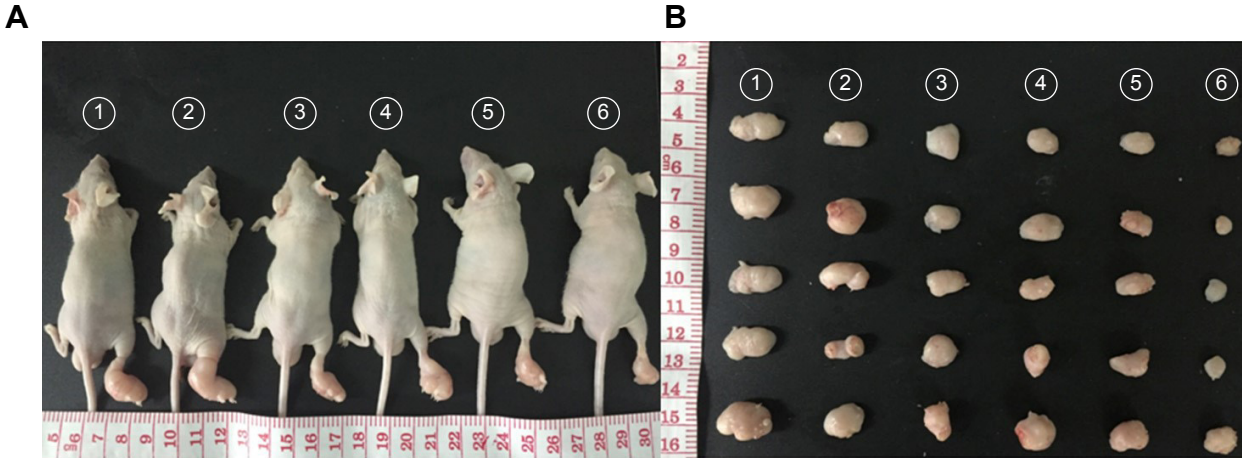

Figure 9 (*Continued*)

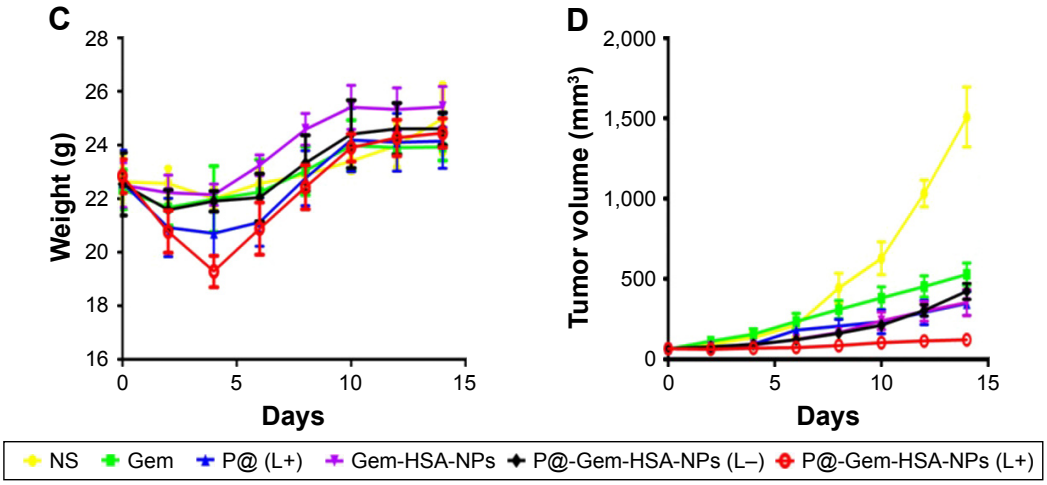

Figure 9 In vivo combined PDT and chemotherapy efficacy assay (Gem equivalent: 50 mg/kg).
Notes: (**A**) Representative photos of tumors on mice in each treatment group. (**B**) Photographs of tumors harvested from each treatment group taken on day 14. (**C**) The body weight profiles of mice in different treatment groups. (**D**) The tumor volume profiles of mice in different treatment groups. 1–6 represent NS group, Gem group, P@ (L+) group, Gem-HSA-NPs group, P@-Gem-HSA-NPs (L–) group, and P@-Gem-HSA-NPs (L+) group, respectively.
Abbreviations: Gem, gemcitabine; HSA, human serum albumin; NPs, nanoparticles; NS, normal saline; P@, pheophorbide-a; PDT, photodynamic therapy.

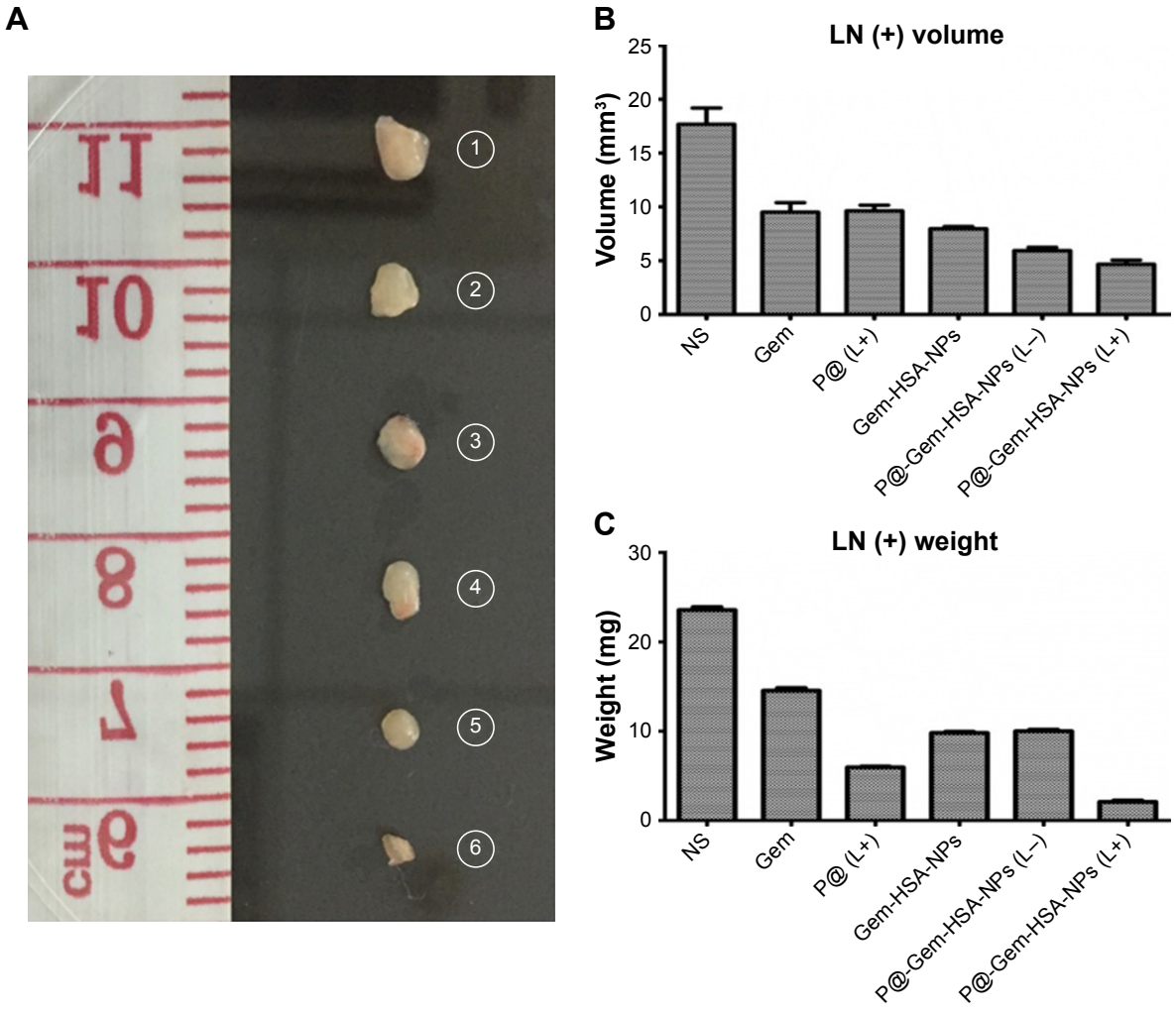

Figure 10 In vivo combined PDT and chemotherapy efficacy assay of metastatic lymph nodes.
Notes: (**A**) Representative photographs of metastatic popliteal lymph nodes harvested from each treatment group taken on day 14. (**B**) The metastatic popliteal lymph node volume profiles of mice in different treatment groups. (**C**) The metastatic popliteal lymph node weight profiles of mice in different treatment groups. 1–6 represent NS group, Gem group, P@ (L+) group, Gem-HSA-NPs group, P@-Gem-HSA-NPs (L–) group, and P@-Gem-HSA-NPs (L+) group, respectively.
Abbreviations: Gem, gemcitabine; HSA, human serum albumin; NPs, nanoparticles; NS, normal saline; P@, pheophorbide-a; PDT, photodynamic therapy.

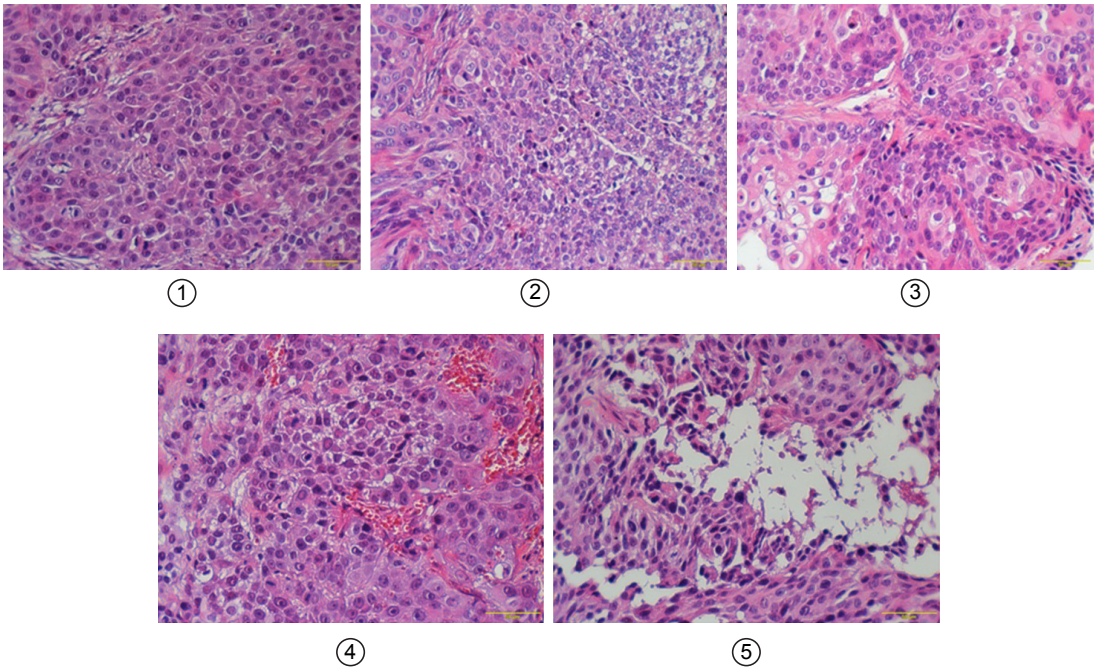

Figure 11 H&E-stained slices of tumors harvested from different groups of mice taken 1 day after IV administration.
Notes: 1–5 represent Gem group, P@ (L+) group, Gem-HSA-NPs group, P@-Gem-HSA-NPs (L–) group, and P@-Gem-HSA-NPs (L+) group, respectively. Bar: 100 μm; magnification ×200.
Abbreviations: Gem, gemcitabine; H&E, hematoxylin and eosin; HSA, human serum albumin; IV, intravenous injection; NPs, nanoparticles; P@, pheophorbide-a.

compared (Figure 11). As noticed, severe damages were noted in the tumor from the combination therapy group (P@-Gem-HSA-NPs [L+]), while no or partial damage could be found in other control groups. Accordingly, the TUNEL staining was used to label apoptotic cells, indicated by red fluorescence in the tumor section (with blue nuclei). As expected, we obtained a parallel result with the above section (Figure 12).

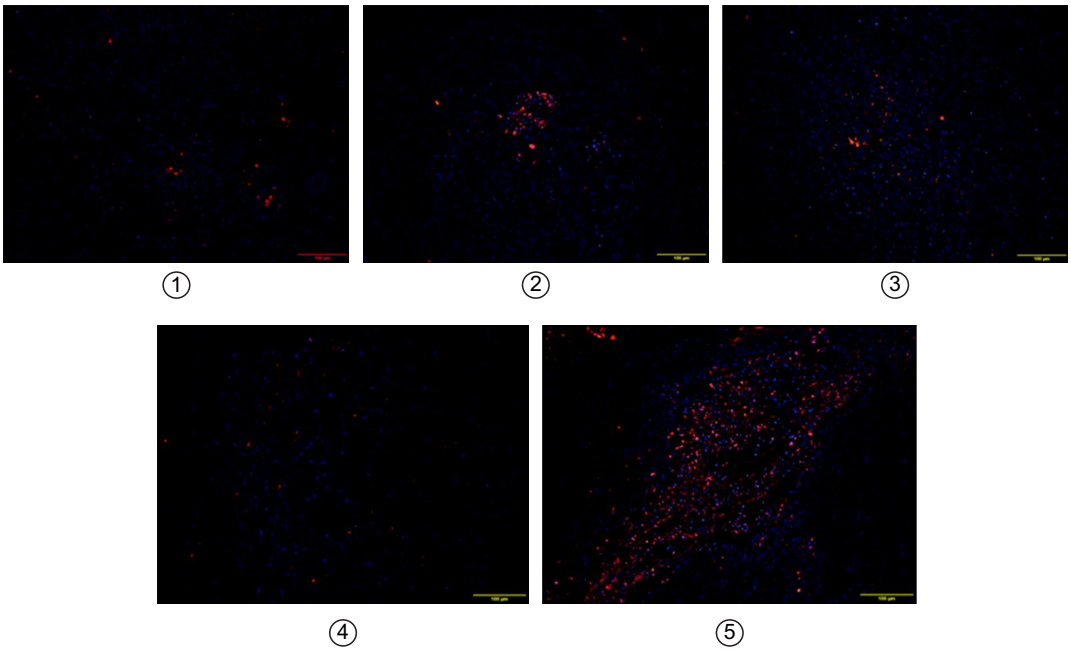

Figure 12 The merged TUNEL stainings showed tumor penetration of drugs on mice-bearing subcutaneous pancreatic tumors on day 1 after IV administration.
Notes: Slices were examined under a confocal microscope. Nuclei were stained with DAPI (blue), while red represents apoptotic cells. 1–5 represent Gem group, P@ (L+) group, Gem-HSA-NPs group, P@-Gem-HSA-NPs (L–) group, and P@-Gem-HSA-NPs (L+) group, respectively. Bar: 100 μm; magnification ×100.
Abbreviations: DAPI, 4′,6-diamidino-2-phenylindole; IV, intravenous injection; TUNEL, transferase dUTP nick end labeling.

In this triple-functional system, the HSA coating offers P@-Gem-HSA-NPs great stability in physiological environments, prolonged blood circulation half-life, and biocompatible character. P@ conjugated on the surface of HSA further renders the nanoplatform highly enriched functionalities for both imaging and therapy. In contrast, by anchoring P@ on NPs, the water solubility of P@ was also improved. The combined PDT and chemotherapy delivered by the single agent, P@-Gem-HSA-NPs, resulted in a remarkable antitumor effect. In vivo safety assessment indicated no apparent side effect on mice; the NPs developed here may be a safe yet effective agent in imaging-guided combination cancer therapy.

Conclusion

We have successfully synthesized an albumin-based theranostic NP, P@-Gem-HSA-NP, which could simultaneously monitor drug delivery and inhibit pancreatic cancer with lymphatic metastases by virtue of combined PDT and chemotherapy. Due to the EPR effect, these triple-functional NPs can selectively accumulate within the primary tumors and metastatic lymph nodes. Just as our study showed, the P@-Gem-HSA-NPs not only serve as imaging probes for the early diagnosis and drug delivery detection but also effectively being served as PDT agents. In addition, with chemotherapy agent Gem being controlled released, a remarkable combined therapeutic effect toward pancreatic cancer with lymphatic metastases has been observed both in vitro and in vivo. Therefore, P@-Gem-HSA-NPs developed in this work may be a safe and rather promising agent for the imaging-guided theranostic of pancreatic cancer with lymphatic metastases.

Acknowledgments

This work was financially supported by the National Natural Science Foundation of China (81472221), Key Project of National Health and Planning Commission of the PRC on General Surgery 2012–2014, Key Project of National Health and Planning Commission of the PRC on Oncology 2013–2015, and the Research Fund for the Doctoral Program of Higher Education of China (20130071110052 and 20110071110065). We declare that we have no financial and personal relationships with other people or organizations that can inappropriately influence our work; there is no professional or other personal interest of any nature or kind in any product, service, and/or company that could be construed as influencing the position presented in, or the review of, the manuscript entitled. In terms of all tables and figures we submitted, we want to make a formal declaration that we confirm all figures and tables are original.

Disclosure

The authors report no conflicts of interest in this work.

References

1. Chen W, Zheng R, Baade PD, et al. Cancer statistics in China, 2015. *CA Cancer J Clin*. 2016;66(2):115–132.
2. Siegel RL, Miller KD, Jemal A. Cancer statistics, 2016. *CA Cancer J Clin*. 2016;66(1):7–30.
3. Ryan DP, Hong TS, Bardeesy N. Pancreatic adenocarcinoma. *N Engl J Med*. 2014;371(11):1039–1049.
4. Su S, Ding Y, Li Y, Wu Y, Nie G. Integration of photothermal therapy and synergistic chemotherapy by a porphyrin self-assembled micelle confers chemosensitivity in triple-negative breast cancer. *Biomaterials*. 2016;80:169–178.
5. Yu X, Li H, Fu D, Jin C, Li JI. Characterization of the role of the photosensitizer, deuteporfin, in the detection of lymphatic metastases in a pancreatic cancer xenograft model. *Oncol Lett*. 2015;10(3):1430–1436.
6. Chu M, Hai W, Zhang Z, et al. Melanin nanoparticles derived from a homology of medicine and food for sentinel lymph node mapping and photothermal in vivo cancer therapy. *Biomaterials*. 2016;91:182–199.
7. Chen Q, Liang C, Wang X, He J, Li Y, Liu Z. An albumin-based theranostic nano-agent for dual-modal imaging guided photothermal therapy to inhibit lymphatic metastasis of cancer post surgery. *Biomaterials*. 2014;35(34):9355–9362.
8. Yu X, Yao L, Di Y, et al. Application of deuteporfin in the metastatic lymph node mapping of pancreatic cancer: an in vivo study. *Photochem Photobiol*. 2016;92(2):325–330.
9. Chen Q, Ke H, Dai Z, Liu Z. Nanoscale theranostics for physical stimulus-responsive cancer therapies. *Biomaterials*. 2015;73:214–230.
10. Chen Q, Wang X, Wang C, Feng L, Li Y, Liu Z. Drug-induced self-assembly of modified albumins as nano-theranostics for tumor-targeted combination therapy. *ACS Nano*. 2015;9(5):5223–5233.
11. Vu-Quang H, Vinding MS, Nielsen T, Ullisch MG, Nielsen NC, Kjems J. Theranostic tumor targeted nanoparticles combining drug delivery with dual near infrared and 19F magnetic resonance imaging modalities. *Nanomedicine*. 2016;12(7):1873–1884.
12. Song X, Liang C, Gong H, Chen Q, Wang C, Liu Z. Photosensitizer-conjugated albumin-polypyrrole nanoparticles for imaging-guided in vivo photodynamic/photothermal therapy. *Small*. 2015;11(32):3932–3941.
13. Chen Q, Wang C, Cheng L, He W, Cheng Z, Liu Z. Protein modified upconversion nanoparticles for imaging-guided combined photothermal and photodynamic therapy. *Biomaterials*. 2014;35(9):2915–2923.
14. Cheng L, Wang C, Feng L, Yang K, Liu Z. Functional nanomaterials for phototherapies of cancer. *Chem Rev*. 2014;114(21):10869–10939.
15. Lucky SS, Soo KC, Zhang Y. Nanoparticles in photodynamic therapy. *Chem Rev*. 2015;115(4):1990–2042.
16. Jiang C, Cheng H, Yuan A, Tang X, Wu J, Hu Y. Hydrophobic IR780 encapsulated in biodegradable human serum albumin nanoparticles for photothermal and photodynamic therapy. *Acta Biomater*. 2015;14:61–69.
17. Song X, Zhang R, Liang C, Chen Q, Gong H, Liu Z. Nano-assemblies of J-aggregates based on a NIR dye as a multifunctional drug carrier for combination cancer therapy. *Biomaterials*. 2015;57:84–92.
18. Zhang J, Liang YC, Lin X, et al. Self-monitoring and self-delivery of photosensitizer-doped nanoparticles for highly effective combination cancer therapy in vitro and in vivo. *ACS Nano*. 2015;9(10):9741–9756.
19. Lee GY, Qian WP, Wang L, et al. Theranostic nanoparticles with controlled release of gemcitabine for targeted therapy and MRI of pancreatic cancer. *ACS Nano*. 2013;7(3):2078–2089.

20. Wang L, An Y, Yuan C, et al. GEM-loaded magnetic albumin nanospheres modified with cetuximab for simultaneous targeting, magnetic resonance imaging, and double-targeted thermochemotherapy of pancreatic cancer cells. *Int J Nanomedicine*. 2015;10:2507–2519.
21. Yu X, Di Y, Xie C, et al. An in vitro and in vivo study of gemcitabine-loaded albumin nanoparticles in a pancreatic cancer cell line. *Int J Nanomedicine*. 2015;10:6825–6834.
22. Liu J, Yang Y, Zhu W, et al. Nanoscale metal-organic frameworks for combined photodynamic & radiation therapy in cancer treatment. *Biomaterials*. 2016;97:1–9.
23. Wang X, Liu K, Yang G, et al. Near-infrared light triggered photodynamic therapy in combination with gene therapy using upconversion nanoparticles for effective cancer cell killing. *Nanoscale*. 2014;6(15):9198–9205.
24. Zhang R, Cheng K, Antaris AL, et al. Hybrid anisotropic nanostructures for dual-modal cancer imaging and image-guided chemo-thermo therapies. *Biomaterials*. 2016;103:265–277.
25. Sun C, Wen L, Zeng J, et al. One-pot solventless preparation of PEGylated black phosphorus nanoparticles for photoacoustic imaging and photothermal therapy of cancer. *Biomaterials*. 2016;91:81–89.
26. Li W, Zheng C, Pan Z, et al. Smart hyaluronidase-actived theranostic micelles for dual-modal imaging guided photodynamic therapy. *Biomaterials*. 2016;101:10–19.
27. Zhou H, Qian W, Uckun FM, et al. IGF1 receptor targeted theranostic nanoparticles for targeted and image-guided therapy of pancreatic cancer. *ACS Nano*. 2015;9(8):7976–7991.
28. Di Corato R, Bealle G, Kolosnjaj-Tabi J, et al. Combining magnetic hyperthermia and photodynamic therapy for tumor ablation with photoresponsive magnetic liposomes. *ACS Nano*. 2015;9(3):2904–2916.
29. Zhong Y, Wang C, Cheng R, et al. cRGD-directed, NIR-responsive and robust AuNR/PEG-PCL hybrid nanoparticles for targeted chemotherapy of glioblastoma in vivo. *J Control Release*. 2014;195:63–71.
30. Yen HC, Cabral H, Mi P, et al. Light-induced cytosolic activation of reduction-sensitive camptothecin-loaded polymeric micelles for spatiotemporally controlled in vivo chemotherapy. *ACS Nano*. 2014;8(11):11591–11602.
31. Yu Z, Li H, Zhang LM, Zhu Z, Yang L. Enhancement of phototoxicity against human pancreatic cancer cells with photosensitizer-encapsulated amphiphilic sodium alginate derivative nanoparticles. *Int J Pharm*. 2014;473(1–2):501–509.
32. Nafiujjaman M, Revuri V, Nurunnabi M, Cho KJ, Lee YK. Photosensitizer conjugated iron oxide nanoparticles for simultaneous in vitro magneto-fluorescent imaging guided photodynamic therapy. *Chem Commun (Camb)*. 2015;51(26):5687–5690.
33. Oh IH, Min HS, Li L, et al. Cancer cell-specific photoactivity of pheophorbide a-glycol chitosan nanoparticles for photodynamic therapy in tumor-bearing mice. *Biomaterials*. 2013;34(27):6454–6463.
34. Cho H, Li L, Bae YH, Huh KM, Kang HC. Bioreducible branched polyethyleneimine derivatives physically loaded with hydrophobic pheophorbide A: preparation, characterization, and light-induced cytotoxicity. *Macromol Biosci*. 2014;14(10):1483–1494.
35. Yu X, Jin C. Application of albumin-based nanoparticles in the management of cancer. *J Mater Sci Mater Med*. 2016;27(1):4.
36. Chen Q, Liu Z. Albumin carriers for cancer theranostics: a conventional platform with new promise. *Adv Mater*. 2016;28(47):10557–10566.
37. Sheng Z, Hu D, Zheng M, et al. Smart human serum albumin-indocyanine green nanoparticles generated by programmed assembly for dual-modal imaging-guided cancer synergistic phototherapy. *ACS Nano*. 2014;8(12):12310–12322.
38. Feng Q, Zhang Y, Zhang W, et al. Tumor-targeted and multi-stimuli responsive drug delivery system for near-infrared light induced chemo-phototherapy and photoacoustic tomography. *Acta Biomater*. 2016;38:129–142.
39. Wang L, Yuan Y, Lin S, et al. Photothermo-chemotherapy of cancer employing drug leakage-free gold nanoshells. *Biomaterials*. 2016;78:40–49.
40. Wang Y, Zhao R, Wang S, Liu Z, Tang R. In vivo dual-targeted chemotherapy of drug resistant cancer by rationally designed nanocarrier. *Biomaterials*. 2016;75:71–81.
41. Yu X, Song Y, Di Y, He H, Fu D, Jin C. Enhanced tumor targeting of cRGD peptide-conjugated albumin nanoparticles in the BxPC-3 cell line. *Sci Rep*. 2016;6:31539.
42. Lee IC, Ko JW, Park SH, et al. Comparative toxicity and biodistribution of copper nanoparticles and cupric ions in rats. *Int J Nanomedicine*. 2016;11:2883–2900.

Supplementary materials

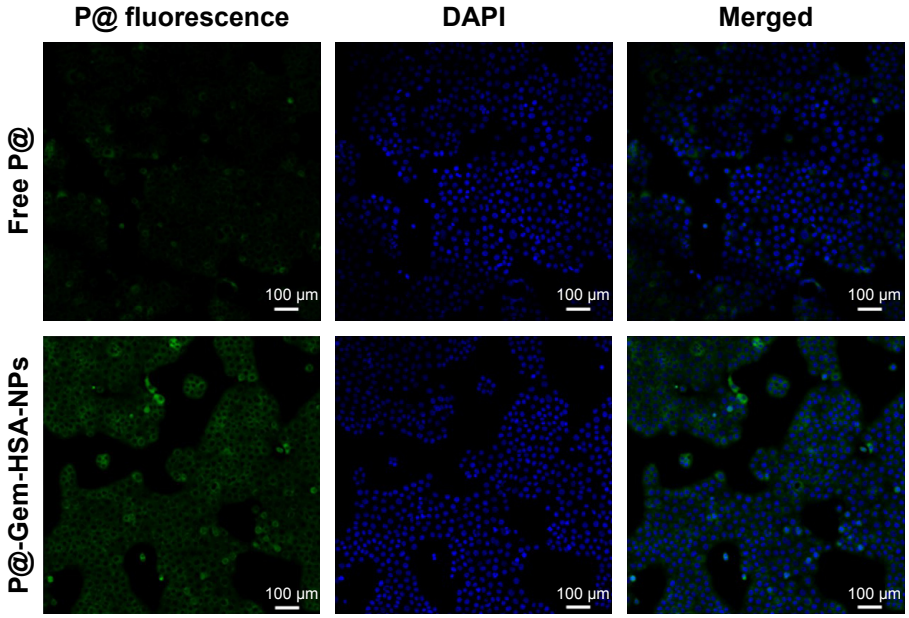

Figure S1 Confocal images of the BxPC-3 cells incubated with free P@ and P@-Gem-HSA-NPs.
Notes: Green: fluorescence of free P@ and P@-Gem-HSA-NPs. Blue: DAPI for BxPC-3 cell nucleus. Merged: fluorescence (green) and DAPI (blue). Bar: 100 μm.
Abbreviations: DAPI, 4′,6-diamidino-2-phenylindole; Gem, gemcitabine; HSA, human serum albumin; NPs, nanoparticles; P@, pheophorbide-a.

Table S1 Serum biochemistry parameters of C57BL/6 mice 10 days after various treatments

Serum biochemistry data	Gem	P@-Gem-HSA-NPs	NS	*P*-value
WBC (10^9/L)	5.2±0.7	4.7±0.4	4.9±0.1	>0.05
RBC (10^{12}/L)	9.8±0.4	9.5±0.7	9.6±0.3	>0.05
HGB (g/L)	148.8±6.1	142.5±7.3	143.0±6.8	>0.05
PLT (10^9/L)	1,399.5±87.2	1,420.3±114.1	1,398.0±50.4	>0.05
ALT (U/L)	30.5±6.6	29.8±10.1	27.1±2.4	>0.05
BUN (mmol/L)	7.2±1.3	6.8±1.4	7.4±0.3	>0.05

Abbreviations: ALT, alanine aminotransferase; BUN, blood urea nitrogen; Gem, gemcitabine; HGB, hemoglobin; HSA, human serum albumin; NPs, nanoparticles; NS, normal saline; P@, pheophorbide-a; PLT, platelets; RBC, red blood cell; WBC, white blood cell.

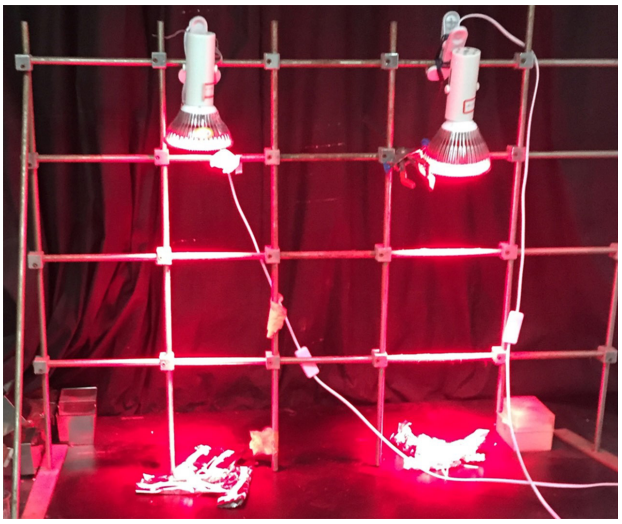

Figure S2 Photo of external NIR emitter with a power density of 10 mW/cm^2.
Note: The irradiation length is 50 cm.
Abbreviation: NIR, near infrared.

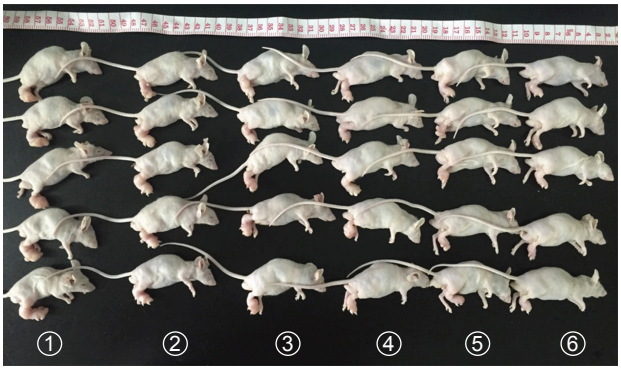

Figure S3 The family portrait of all mice in different treatment groups on day 14 postinjection.
Note: 1–6 represent NS group, Gem group, P@ (L+) group, Gem-HSA-NPs group, P@-Gem-HSA-NPs (L–) group, and P@-Gem-HSA-NPs (L+) group, respectively.
Abbreviations: Gem, gemcitabine; HSA, human serum albumin; NPs, nanoparticles; NS, normal saline; P@, pheophorbide-a.